Phonons on stepped surfaces

P. Knipp*
Department of Physics and The James Franck Institute, The University of Chicago, Chicago, Illinois 60637
(Received 16 July 1990)

A simple model of fcc lattice dynamics is studied in the vicinity of a clean, unreconstructed, high-Miller-index (i.e., stepped) surface. Depending on the vibrational modes' spatial extent, they are classified as either bulk phonons, surface phonons, or step phonons. The existence and characteristics of the latter class of vibrational modes are presented throughout the (one-dimensional) step Brillouin zone (BZ). Five classes of stepped surfaces are examined, each differing in the Miller indices of the terrace [(111) or (100)] and step face [(111), (100), or (110)]. All but one of the systems exhibit modes truly localized to the edge. There are many similarities to the study of *surface* phonons. For instance, when degenerate with the bulk- or surface-phonon bands, the step phonons acquire a finite lifetime and become step resonances. A total of seven step phonons and four step resonances are seen. Most of these are strongly localized to the edge only near the end of the step BZ. Unlike regular surface modes, the step-phonon characteristics (frequency, polarization, and amplitude) depend sensitively on the interatomic potentials near the steps. Two step-phonon measurements have yielded information about these important step parameters. Using a crude estimate of the inelastic-scattering intensity, I propose the possibility for a similar experiment with Ni(755) using existing techniques.

I. INTRODUCTION

Surfaces figure prominently in such phenomena as catalysis, nucleation, and crystal growth. Understanding the energy transfer in such processes requires a detailed knowledge of the phonons. In particular, a localized vibrational mode might catalyze a reaction which is otherwise thermodynamically suppressed.[1] In certain circumstances, stepped surfaces are considerably more reactive than their flat counterparts. This may be because adparticles diffuse freely across terraces until sticking on a step, leading to high effective concentrations of reagents. In other circumstances, the limited mobility of atoms adsorbed on a step might *decrease* the reactivity, compared to a flat surface. Hence step vibrations are crucial in nonequilibrium processes at surfaces.

Vibrations of flat surfaces have been studied extensively. By comparing these with bulk phonons, one learns how closely the surface interatomic potentials resemble their interior counterparts. This has been done for a number of low-Miller-index (MI) surfaces [i.e., (111), (100), and (110) planes]. The experimental methods usually consist of either electron energy-loss spectroscopy[2] (EELS) or inelastic helium-atom scattering (HAS).[3,4] To extract information about surface properties, the energy-loss spectra must be compared with theoretical predictions. The theoretical methods involve either molecular-dynamics simulations or, in the harmonic approximation, ball-and-spring models whose Hamiltonian is diagonalized by standard techniques of linear algebra.[5,6] Nontrivial inputs to either of these procedures require preliminary estimates of the interatomic potentials, obtained either empirically or from first principles. For low-MI surfaces, a few (~ 3) vibrational modes propagate freely parallel to the surface but decay exponentially into the crystal interior. A general tenet of wave mechanics asserts that the presence of a defect is a necessary but not sufficient condition for the existence of one (or more) localized mode. If viewed as a defect, a surface is strong enough to localize vibrational modes,[7] commonly referred to as surface phonons.

Near a surface, the bonding coordination number is greatly reduced from the near-isotropic situation existing in the bulk. This perturbation induces electronic charge redistribution which may in turn substantially alter the interatomic potential. Numerical studies show the characteristics of surface modes (i.e., their frequency, polarization, and amplitude) to depend strongly on the surface interatomic potential. For instance, stiffening (softening) force constants near a surface tends to increase (decrease) surface-phonon frequencies. This effect is enhanced if the mode is strongly localized in the surface layer, and specific details of these deviations are governed by the phonon polarization. Careful analysis of surface-phonon spectra (frequencies *and* intensities) can yield substantial information about interatomic-potential modifications induced by a surface.

Studies of *high*-MI (also known as vicinal or stepped) surfaces have been hampered by the complex assortment of surface phonons that exist on them, in addition to other experimental and theoretical difficulties. At fixed wave vector, the number of surface modes increases (roughly) linearly with the surface unit cell area—i.e., proportional to the (maximum) MI.[8] This greatly complicates the spectrum. However, advances have been made in recent experimental and theoretical studies of surfaces with unkinked steps. The surface phonons divide into two classes. The first class is characteristic of the terrace and consists of surface phonons reflected and transmitted by the step edges.[9,10] Features of these surface phonons are

well approximated by folding the (two-dimensional) Brillouin zone (BZ) of the terrace. The second class, considerably smaller in number, is localized at the edges, along which they propagate freely.[11] This class had been known to exist theoretically for macroscopic steps,[12] and experimentally for two systems with monatomic steps,[10,13] but had escaped verification for monatomic steps of crystals with simple force-constant models.[14] Near a step, further reduction of atomic coordination induces even more charge-density redistribution and a more substantially altered interatomic potential than for a flat surface. Unlike ordinary surface phonons, the characteristics of step phonons are strongly sensitive to changes in the near-*step* force constants, as will be seen in Sec. V E. Hence the measurement of these vibrational modes yields information about an important region of the crystal.

One might view that the relationship of a step to the surface is the same as that of a surface to the bulk. Indeed, an isolated kink in a straight step on an otherwise flat surface further decreases the dimensionality of the translational periodicity (Fig. 1), thereby allowing for the possibility of kink modes, vibrations localized in all three directions. These modes are not expected to exist for the simple model to be used here, as discussed in the Appendix; therefore vibrations near kinks are not investigated in this paper. To appreciate the differing dimensionalities of these phonons, consider the aftereffects of a microscopic disturbance (e.g., an impinging gas particle) near a kink on a surface. Quantitative description of this would require arduous calculation, but qualitative aspects are easily derived from geometrical considerations. Depending on the initial spatial dependence of the disturbance, the energy propagates away via four simultaneous mechanisms, in comparable proportions. First, bulk waves propagate away into a solid angle of 2π sr. Conservation of energy mandates that the intensity (i.e., squared amplitude) of these bulk modes decrease with distance as $1/R^2$. Second, surface waves propagate into the terraces, decreasing in intensity as $1/R$. (Macroscopically, these are earthquake waves.) Third, step modes propagate away in two opposite directions, the intensity not diminishing at all (at least not algebraically) with R. Finally, certain amounts of the initial energy will not propagate, remaining instead as kink modes. Eventually, anharmonic effects will perturb this noninteracting-phonon picture, causing all of the energy to propagate into the crystal interior as bulk phonons, thereby establishing thermal equilibrium between the kink, the step, the surface, and the interior.

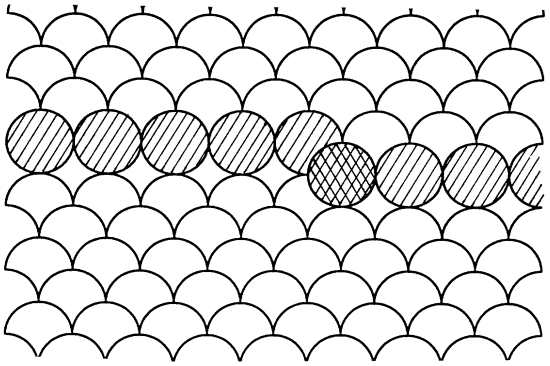

FIG. 1. Oblique view of an isolated kink in a step on an otherwise flat surface, to be contrasted with the unkinked step in Fig. 2(a). Singly hatched circles and the cross-hatched circle represent edge atoms and the kink atom, respectively.

Section II describes the geometries of five classes of stepped surfaces covered here, in real space and momentum space. Section III discusses the simple lattice-dynamics model used, as well as the different types of spectral-density functions necessary for the description of vibrations near an isolated step on an otherwise flat surface. Section IV presents the bands of bulk and surface phonons relevant to these systems, and the method of numerical calculation for the step phonons. The fairly simple results in Sec. V demonstrate infinite-terrace-width behavior for the vibrations of vicinal surfaces whose terraces are only a few angstroms wide. Section V also shows the dependence of step modes upon realistic deviations of the force-constant model, thereby demonstrating the step sensitivity of any experiment which could detect such modes. Section VI summarizes the only two step-phonon measurements to date and also proposes a third such experiment, for Ni(755). Finally, Sec. VII contains conclusions of these results.

II. GEOMETRY

A stepped surface is easily constructed by slicing a single crystal at an orientation differing slightly from a low-MI plane. This paper restricts itself to monatomic fcc lattices with five of the simplest step environments, represented graphically in Figs. 2(a)–2(e) and mathematically in Table I.

TABLE I. Stepped fcc surfaces covered in this paper. Key for last column (see Fig. 7 of this paper or Fig. 1 of Ref. 5): CR is centered rectangular, PR is primitive rectangular, and PO is primitive oblique.

	Terrace	Step edge	Step face	Vicinal surface Miller index ($N \gg n > 0$)	Approximate terrace width (interatomic spacings)	Shape of Brillouin zone
A	(111)	$[1\bar{1}0]$	(001)	$(N\,N\,N+n)$	$\sqrt{3}N/n$	PR or CR
B	(111)	$[1\bar{1}0]$	$(11\bar{1})$	$(N\,N\,N-n)$	$\sqrt{3}N/n$	PR or CR
C	(111)	$[2\bar{1}\,\bar{1}]$	$(01\bar{1})$	$(N\,N+n\,N-n)$	N/n	PO
D	(100)	$[01\bar{1}]$	(111)	$(N\,n\,n)$	$N/2n$	CR
E	(100)	[001]	(110)	$(N\,n\,0)$	$N/\sqrt{2}n$	PR or CR

To better appreciate the similarities and differences between these classes of vicinal surfaces, a few details are worth emphasizing. First, the (111) and (100) surfaces are the first- and second-most tightly packed fcc surfaces (Fig. 3). The terraces of the stepped surfaces studied here are of either one type (A,B,C) or the other (D,E). Second, the $[1\bar{1}0]$ direction connects nearest neighbors so yields a straight step edge. On the other hand, a $[\bar{2}11]$ edge on a (111) surface or a [001] edge on a (100) surface are kinked. Both straight (A,B,D) and kinked (C,E) steps are investigated herein. Third, since the $[1\bar{1}0]$ direction does not parallel a reflection plane of fcc(111), there exist two different ways of constructing such a monatomic step (Fig. 4) yielding step faces with MI's (001) or $(11\bar{1})$. Both of these (A,B) are discussed here.

For reasons of computational practicality, it is useful to avoid vicinal surfaces with nonuniformly sized terraces. Using the A-type system as an example, fcc(113) and fcc(112) have one and two atomic rows, respecitvely, in all of their terraces. However, fcc(337) has terraces whose widths *alternate* in size between one and two rows. The undesirability of this trait (to be detailed at the end of Sec. IV) leads to the imposition of further restrictions upon the MI's. For A-, B-, and C-type surfaces, n is restricted to 1 or 2 (see Table I). For D types, N is odd and n equals unity. Lastly, n equals unity for type-E systems. The BZ shapes listed in the last column of Table I reflect these restriction.

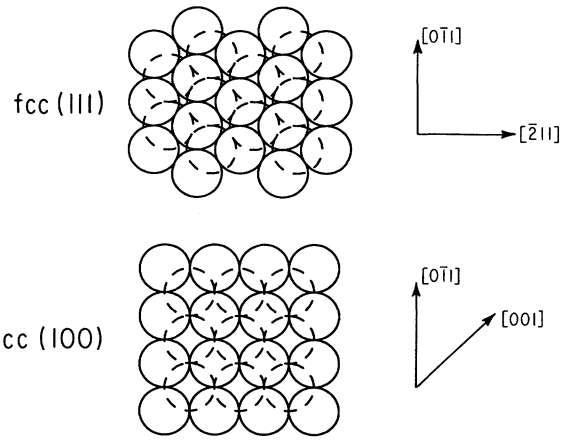

FIG. 3. Top views of surface atoms of fcc(111) and fcc(100), with dashed circles representing second layer atoms.

The MI (h,k,l) of a crystal surface can be put into a one-to-one correspondence with the unit sphere using the transformation

$$(h^2+k^2+l^2)^{-1/2}(h,k,l)=(\sin\theta\cos\phi,\sin\theta\sin\phi,\cos\theta)\ ,$$

a common way to represent surface orientation. For cubic crystals, the irreducible element of the unit sphere is the stereographic triangle (Fig. 5), whose corners correspond to the three lowest MI surfaces: (111), (100), and (110). The surfaces discussed here lie near either the (111) or (100) vertex of this triangle. Of the five types of step, four lie on the boundary and one occupies the interior of the triangle. Two other common methods for repre-

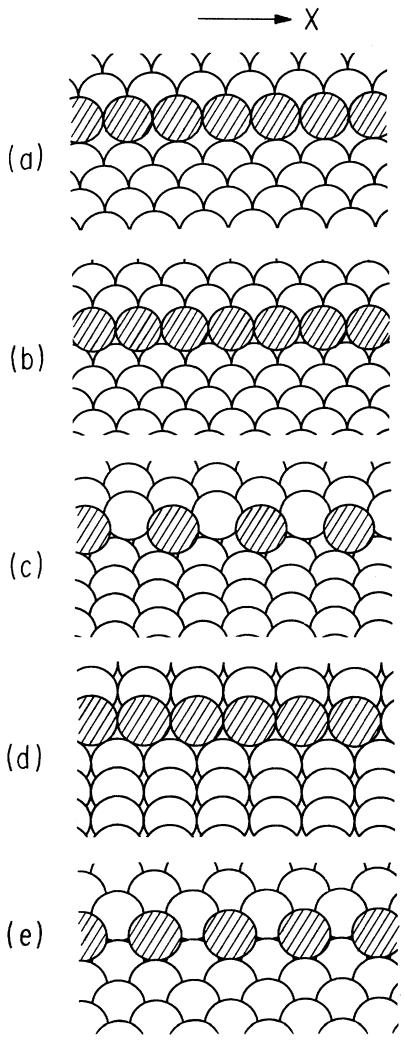

FIG. 2. Oblique view of steps $A-E$ are presented in (a)–(e), respectively. Hatched circles represent edge atoms.

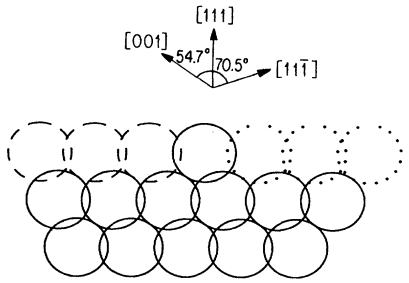

FIG. 4. Cross section of fcc(111), with $[1\bar{1}0]$ direction pointing into the page. Removing dashed circles creates a (001) step face (A) whereas removing dotted circles creates a $(11\bar{1})$ step face (B).

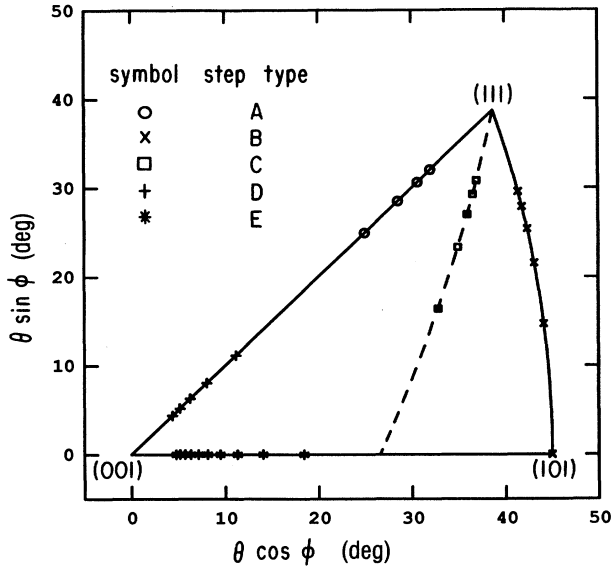

FIG. 5. Stereographic triangle, which contains representations of all cubic crystal surfaces. Symbols depict specific surfaces investigated in Sec. V, and dashed line is the locus of all type-*C* stepped surfaces.

sentation of high-MI surfaces are microfacet notation[15] and a nomenclature which specifies the (small) angle between the vicinal surface and a low-MI plane.[16]

That these vicinal surfaces often reconstruct has been detected by techniques sensitive to surface structure, such as low-energy electron diffraction (LEED), elastic helium scattering, and x-ray diffraction. This crystalline rearrangement, which would make irrelevant many of the results in this paper, occurs in one of two ways. First, the steps might attract each other and combine to form polyatomic steps. Second, the steps might form polyatomic kinks, thereby increasing their total edge length. A stepped surface which does not reconstruct when clean might do so if covered with a small amount of light atoms.[15] Sometimes the opposite occurs, in that adsorbates *stabilize* a surface which otherwise reconstructs.[16] In addition, these phenomena often depend upon the temperature. Phase diagrams for vicinal surfaces have been studied, perhaps none more thoroughly than for platinum, for which only *E*-type steps reconstruct.[15] For nickel, *B*-type surfaces reconstruct, whereas those of type *A* do not.[16]

Unreconstructed vicinal surfaces are periodic in both the $\hat{\mathbf{x}}$ (parallel to the step) direction and the $\hat{\mathbf{y}}(\perp\hat{\mathbf{x}})$ direction, but the period in the latter direction greatly exceeds 1 Å. Hence the surface BZ more closely resembles a line segment than a polygon (Fig. 6). An isolated step on an otherwise flat surface has only one periodic translational symmetry, thereby yielding a truly one-dimensional BZ, indicating that step modes propagate in only one direction. The length of the step BZ varies inversely with the periodicity along the step, so surfaces with [011] edges (*A*,*B*,*D*) have the longest BZ (with length $Q_{\max}=\pi/r_0$, where r_0 is the interatomic spacing). On the other hand, the kinks on steps *C* and *E* result in BZ lengths $\pi/\sqrt{3}r_0$ and $\pi/\sqrt{2}\pi_0$, respectively (Fig. 7). The thin BZ's of the surfaces discussed in this paper are of three slightly different shapes, as illustrated in Fig. 7 and denoted in the last column of Table I.

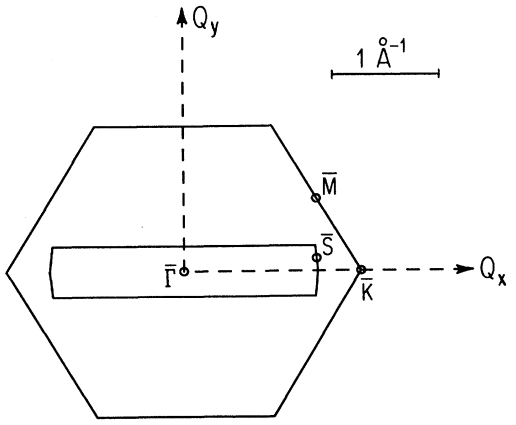

FIG. 6. Surface BZ's for Ni(111) (hexagon) and Ni(755).

III. THEORY

The equation of motion for the displacements $\mathbf{u}(l)$ of the atoms away from equilibrium is derived from the Hamiltonian H, represented in the harmonic approximation as

$$H(\mathbf{u}(l_1),\mathbf{u}(l_2),\ldots)=H_0+\sum_{\alpha,l}u_\alpha(l)\frac{\partial\Phi}{\partial u_\alpha(l)}+\tfrac{1}{2}\sum_{\alpha,\beta,l,l'}u_\alpha(l)u_\beta(l')\times\frac{\partial^2\Phi}{\partial u_\alpha(l)\partial u_\beta(l')}\,, \quad (1)$$

where H_0 includes the kinetic energy and the zero of the

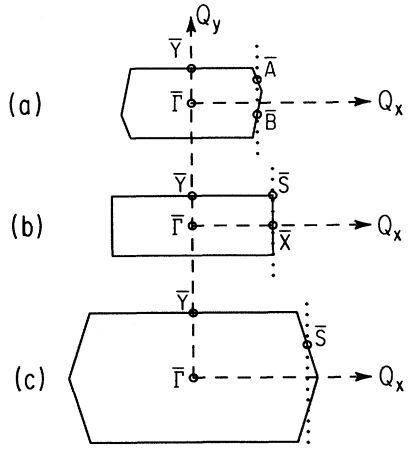

FIG. 7. Examples of the three differently shaped surface BZ's for systems studied here: (a) fcc(342), a *C*-type stepped surface, with a *p*-oblique BZ; (b) fcc(510), an *E*-type system with a *p*-rectangular BZ; and (c) fcc(511), a *D*-type surface, with a *c*-rectangular BZ. Circles indicate high-symmetry points of the surface BZ, and dots delineate the "end" of the *step* BZ.

potential energy. The function $\Phi(\mathbf{u}(l_1),\mathbf{u}(l_2),\ldots)$ is the adiabatic many-atom potential, the subscript α or β specifies one of three Cartesian directions, and the vector $l=(l_x,l_y,l_z)$ has integral components in a convenient, nonorthogonal basis. The single index l_z specifies a *layer* of atoms parallel to the surface. In the harmonic approximation, quantum and classical results coincide. The second term in Eq. (1) vanishes, owing to the equilibrium condition that $Md^2u_\alpha(l)/dt^2=-\partial\Phi/\partial u_\alpha(l)=0$, where M is the atomic mass.

To emphasize the generality of the results to be presented in this paper, a very basic model of lattice dynamics is used. Later, step-phonon sensitivity to various deviations from this model is tested. I restrict the many-body potential to a sum of central two-body potentials:

$$\Phi(\mathbf{u}(l_1),\mathbf{u}(l_2),\ldots)=\tfrac{1}{2}\sum_{l,l'}\phi(|\mathbf{r}(l)+\mathbf{u}(l)-\mathbf{r}(l')-\mathbf{u}(l')|)\ ,$$

where $\mathbf{r}(l)$ is the equilibrium position of the lth atom. An additional assumption is that $\phi(|\mathbf{R}|)$ vanishes for all but the (12) nearest neighbors of each atom. This leads to the following force-constant matrix:

$$\frac{\partial^2\Phi}{\partial u_\alpha(l)\partial u_\beta(l')}=\begin{cases}\left[\dfrac{\phi'}{r_0}-\phi''\right]n_\alpha n_\beta-\dfrac{\phi'}{r_0}\delta_{\alpha\beta} & \text{if } l \text{ and } l' \text{ are nearest neighbors}\\ 4\left[\phi''+2\dfrac{\phi'}{r_0}\right]\delta_{\alpha\beta} & \text{if } l=l'\ ,\\ 0 & \text{otherwise}\ ,\end{cases} \tag{2}$$

where $\mathbf{n}=[\mathbf{r}(l)-\mathbf{r}(l')]/|\mathbf{r}(l)-\mathbf{r}(l')|$. The derivatives on the right side of Eq. (2) are evaluated at $|\mathbf{R}|=r_0$. Often, ϕ'/r_0 and ϕ'' are referred to as the tangential force constant and the radial- or bond-stretching force constant, respectively. In the bulk, energy minimization requires that $\phi'=0$ (but this constraint might be lifted near a surface or step, as will be done in Sec. V E).

By tuning the one free parameter ϕ'', this model does a reasonably good job of fitting measured bulk-phonon characteristics for a large number of fcc materials (see, e.g., Fig. 1 of Ref. 17), yielding a maximum phonon frequency $\omega_{\max}=2\sqrt{2}\sqrt{\phi''/M}$ (=36.6 meV for nickel). Unless otherwise specified, the units for all frequencies (and the inverse of all spectral densities) will be the natural frequency $\sqrt{\phi''/M}$. For simplicity, I hold the crystalline interatomic potential and geometry in the vicinity of terraces unchanged from their bulk values. This does reasonably well at predicting surface-phonon characteristics.[18] The last approximation is that the potential and geometry in the vicinity of *steps* is unchanged from the bulk. These assumptions are not expected to be very reasonable near a step, where the atomic environment differs greatly from both that of the bulk and that of the flat surface. However, in the absence of both *ab initio* calculations of force constants and experimental measurements of near-step geometry, this model generates results which should serve as convenient (and well-defined) reference points for the interpretation of future experiments. This model is identical to that used in Ref. 8, and in fact a lot of the data presented here can be extracted directly from that extensive paper.

Owing to two-dimensional periodicity near a surface, phonons in this region are parametrized by the two-dimensional wave vector $\bar{Q}$. [Throughout this paper, I will use the notation $\mathbf{V}$ to denote a three-dimensional wave vector, $\bar{V}$ to denote its two-dimensional projection onto the surface, and V ($=\bar{V}\cdot\hat{\mathbf{x}}=\mathbf{V}\cdot\hat{\mathbf{x}}\neq|\mathbf{V}|$) to denote their one-dimensional projection along the step edge.] To find the normal modes for each $\bar{Q}$, one must diagonalize the dynamical matrix

$$d_{\alpha\beta}(l_z,l_z';\bar{Q})=M^{-1}\sum_{\bar{l}'}\frac{\partial^2\Phi}{\partial u_\alpha(l)\partial u_\beta(l')}\exp i\bar{Q}\cdot\mathbf{r}(l-l')\ . \tag{3}$$

All relevant information about phonons near surfaces is contained in the spectral-density function

$$\rho_{\alpha\beta}(l_z,l_z';\bar{Q},\omega)=\sum_n e_\alpha^{(n)}(l_z,\bar{Q})[e_\beta^{(n)}(l_z',\bar{Q})]^*\times\delta(\omega-\omega_n(\bar{Q}))\ , \tag{4}$$

where $e_\alpha^{(n)}(l_z,\bar{Q})$ and $\omega_n^2(\bar{Q})$ are the nth eigenvector and eigenvalue, respectively, of the dynamical matrix. The spectral density is simply related to various correlation functions, and additionally appears in formulas for inelastic-scattering intensities in which $\hbar\omega$ and $\hbar\bar{Q}$ represent the energy transfer and parallel-momentum transfer, respectively.[19] Where possible to avoid confusion, explicit reference to the dependence of various quantities upon the subscripts α and β will be omitted. Plots of the spectral density will represent the trace $\mathrm{Tr}\rho(\omega)=\rho_{xx}(\omega)+\rho_{yy}(\omega)+\rho_{zz}(\omega)$.

Surface phonons manifest themselves in $\rho(l_z,l_z';\bar{Q},\omega)$ as δ functions in ω whose integrated strengths decrease rapidly with increasing l_z or l_z' (Fig. 8). When l_z and l_z' are large, $\rho(l_z,l_z')$ depends only on the difference $l_z-l_z'\equiv L_z$, reducing to

$$\rho(l_z,l_z';\bar{Q},\omega)\to\rho(L_z;\bar{Q},\omega)\equiv C_1\int dQ_z\rho(\mathbf{Q},\omega)\exp iQ_z r_z(L_z)\ . \tag{5}$$

The function $\rho(\mathbf{Q},\omega)=\sum_{n=1}^{3}e^{(n)}(\mathbf{Q})e^{(n)*}(\mathbf{Q})\delta(\omega-\omega_n(\mathbf{Q}))$ is the bulk spectral density, which relates

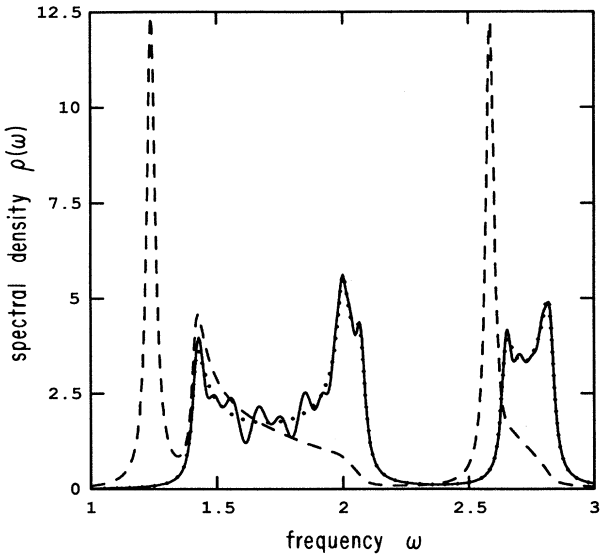

FIG. 8. Surface spectral density of fcc(111) evaluated at $\bar{Q}=\bar{M}$, a high-symmetry point of the surface BZ (dashed line). Also shown is the same spectral density, evaluated 10 layers deep (solid line). The peaks at $\omega=1.24$ (Rayleigh mode S_1) and $\omega=2.59$ ("gap" mode S_2) are due to surface phonons, whereas the two broad bands at $1.41<\omega<2.07$ and $2.66<\omega<2.83$ are due to bulk phonons. By 10 layers, the surface mode peaks have decreased by several orders of magnitude. In fact, the solid line should be compared with the surface-projected bulk spectral density $\rho(L_z;\bar{Q}=\bar{M},\omega)$ (dotted line). These and all subsequent spectra have frequency units of $\sqrt{\phi''/M}$ (=12.9 meV for nickel, as an example) and have been convolved with a Lorentzian whose half width $\Delta\omega$ equals 0.02.

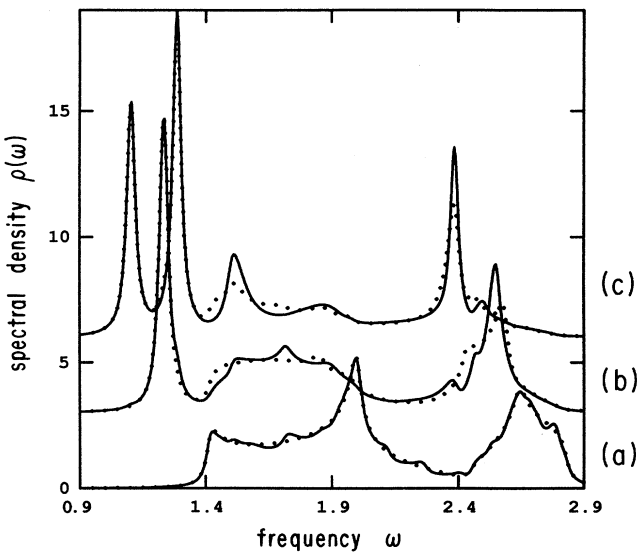

FIG. 9. (a) Edge-projected bulk spectral density $[\rho(L_y=L_z=0;Q,\omega)]$ for fcc(111) with a $[1\bar{1}0]$ edge, evaluated for Q at the end of the step BZ (dotted line). This is compared with the spectral density for fcc(755) for $\bar{Q}=\bar{S}$, evaluated deep inside the crystal (solid line). (b) Edge-projected surface spectral density $[\rho(L_y=0;l_z=l_z'=1;Q,\omega)]$ for fcc(111) with a $[1\bar{1}0]$ edge, evaluated for Q at the boundary of the step BZ (dotted line). This is compared with the spectral density for fcc(755) at $\bar{Q}=\bar{S}$, evaluated in the middle of the terrace (solid line). In addition to the bulk band ($\sqrt{2}\le\omega\le2\sqrt{2}$), the peak at $\omega\sim1.23$ is a (substantially narrower) surface-phonon band. (c) Spectral densities for (211) (solid line) and (755) (dotted line) surfaces, evaluated at the step edge for $\bar{Q}=\bar{S}$. Note the rapid convergence as the terrace width increases from approximately 2 to 5 (atomic rows). The bulk band ($\sqrt{2}\le\omega\le2\sqrt{2}$) is present but the surface band ($1.227\le\omega\le1.241$) is missing at m (or m')=1, signifying that the S_1 amplitude vanishes at the step. The peaks at $\omega=1.10$, 1.28, and 2.38 are due to step phonons. For clarity the three pairs of curves are separated by $\Delta\rho=3.0$.

directly to the energy-loss spectrum of neutrons scattered from a crystal. In this and other similar integrals over one or more wave-vector components, the constants C_j and the range of integration are chosen so that $C_j\int\cdots\int d^nQ$ equals unity. The surface-projected bulk spectral density $\rho(L_z;\bar{Q},\omega)$ contains no surface information but serves two purposes. First, through Eq. (5) it can be compared to the limiting behavior of $\rho(l_z,l_z')$, thereby serving as a check of the numerical calculation (Fig. 8). Second, bulk-phonon bands appearing in $\rho(L_z;\bar{Q},\omega)$ also exist in $\rho(l_z,l_z';\bar{Q},\omega)$, whose knowledge aids the interpretation of features in the surface spectral density.

However, the main task of this paper will not hinge upon the three different spectral-density functions discussed up to here, as these do not allow for the treatment of an isolated step on an otherwise flat surface. Near the step of such a system, the spectral density is more appropriately described by the inclusion of two indices l_y and l_y' which indicate horizontal distance of each atom from the step edge:

$$\rho(l_y,l_z;l_y',l_z';Q,\omega)=\sum_n e^{(n)}(l_y,l_z;Q)[e^{(n)}(l_y',l_z';Q)]^*\times\delta(\omega-\omega_n(Q))\ . \tag{6}$$

The ordered pair (l_y,l_z) specifies a *row* of atoms parallel to the step. Near an edge, step phonons manifest themselves in $\rho(l_y,l_z;l_y',l_z';\omega)$ as δ functions in ω whose integrated strengths decrease rapidly as either l_y, l_y', l_z, or l_z' increase. When l_z and l_z' are large, $\rho(l_y,l_z;l_y',l_z')$ depends only on the pair of differences L_z and $l_y-l_y'\equiv L_y$, thereby reducing to

$$\rho(l_y,l_z;l_y',l_z';Q,\omega)\to\rho(L_y,L_z;Q,\omega)\equiv C_2\int\int dQ_y dQ_z\rho(\mathbf{Q},\omega)\exp\{i[Q_y r_y(\mathbf{L})+Q_z r_z(\mathbf{L})]\}\ . \tag{7}$$

The function $\rho(L_y,L_z;Q,\omega)$ will be called the edge-projected bulk spectral density. Figure 9(a) demonstrates Eq. (7) graphically. If l_y and l_y' are large, $\rho(l_y,l_z;l_y',l_z')$ depends only on l_z, l_z', and L_y, with the simplification

$$\rho(l_y,l_z;l_y',l_z';Q,\omega)\to\rho(L_y;l_z,l_z';Q,\omega)\equiv C_3\int dQ_y\rho(l_z,l_z';\bar{Q},\omega)\exp[iQ_y r_y(\mathbf{L})]\ . \tag{8}$$

Here, $\rho(L_y;l_z,l_z';Q,\omega)$ is the edge-projected surface spectral density. Figure 9(b) verifies the asymptotic behavior asserted by Eq. (8). Only $\rho(l_y,l_z;l_y',l_z')$ contains information about step vibrations. However, the two edge-projected spectral densities $\rho(L_y;l_z,l_z')$ and $\rho(L_y,L_z)$ prove useful for the study of vibrations near steps in much the same way that the *surface*-projected spectral density $\rho(L_z)$ is important for studying surface vibrations, as outlined in the previous paragraph.

The normalization of the functions listed in Table II is determined by their precise definitions and by the completeness relation $\sum_n |n\rangle\langle n| = I$, where $|n\rangle$ is the nth eigenvector of a dynamical matrix. For instance, the normalization of the edge-projected surface spectral density is $\int_0^\infty d\omega\, \rho_{\alpha\beta}(L_y;l_z,l_z';Q,\omega) = \delta_{\alpha\beta}\delta_{l_z l_z'}\delta_{L_y}$.

In addition to step-phonon peaks, the frequency spectrum of $\rho(l_y,l_z;l_y',l_z';Q,\omega)$ contains both bulk- and surface-phonon bands, as will be specifically shown in the next section. Strictly speaking, a step mode exists only if it does not lie in either of these bands. Otherwise, it would couple to these modes, radiate away its energy and amplitude, and be a finite-lived step resonance, in the same way that the excited states of the hydrogen atom are nonstationary, owing to their coupling with the electromagnetic continuum. This also closely parallels the situation for a flat surface, where a surface resonance represents the dissipative coupling of a surface model to a continuous band of bulk modes. On flat crystals, it is possible for surface phonons to be symmetry-decoupled from degenerate bulk bands if the wave vector parallels a mirror plane of the crystal.[5] On stepped crystals, however, the only mirror plane is perpendicular to the step. Hence the only wave vectors which would allow such a decoupling are in a very small neighborhood around $\bar{Q}=\bar{\Gamma}$, the origin of the BZ. Even this is untrue for step C, which has no mirror plane [see Fig. 2(c)].

IV. NUMERICAL DETAILS

The first item of business is to determine the extent (in frequency) of the bands spanned by the edge projection of bulk phonons $\rho(L_y,L_z;Q,\omega)$. The boundaries of the bulk bands for a [110] edge are portrayed in Figs. 10(a), 10(b), and 10(d); for a $[11\bar{2}]$ edge, in Fig. 10(c); and for a [001] edge, in Fig. 10(e). In all three cases the edge-projected bulk band contains no frequency gaps, which contrasts with the familiar gaps in *surface*-projected bulk bands [e.g., Figs. 7(e)–7(g) of Ref. 5].

The next task is to determine the extent of the bands generated by the edge-projection of *surface* vibrations $\rho(L_y;l_z,l_z';Q,\omega)$. Figure 10 depicts the surface-band boundaries for a (111) surface with $(1\bar{1}0)$ edge [10(a) and 10(b)], a (111) surface with $[11\bar{2}]$ edge [10(c)], a (100) surface with [011] edge [10(d)], and a (100) surface with [001] edge [10(e)]. Note that Figs. 10(a) and 10(b) exhibit a gap between the edge-projected surface and bulk bands, albeit a narrow one. This allows for the possibility of step phonons residing within this gap, reminiscent of gap modes on flat surfaces.[5]

The characteristics of phonons near an isolated step are studied by performing calculations for high MI surfaces with such steps. The separation between steps (i.e., the inverse of the angle between the stepped surface and the flat surface) is increased by integral numbers of atomic rows, until the spectral density converges to its infinite-terrace-width limit. Figure 9(c) demonstrates how swiftly this limit is reached. This process resembles slab calculations (see next paragraph), in which the crystal thickness is increased until no substantial change is seen in the *surface*-phonon eigenvectors and frequencies.

The method of calculation was the Green's-function technique, an exact, semianalytic method which allows the crystal to be infinitely thick.[20] This previously used approach has been incorporated into a very general computer program which allows for any force-constant model or surface Miller index. This contrasts with the more commonly used slab technique,[5] which involves brute-force diagonalization of a matrix whose size is proportional to the crystal thickness. For stepped surfaces the slab technique is even more cumbersome, as the size of the matrix becomes proportional to the *product* of the slab thickness and of the distance between step edges. The sizes of the matrices manipulated by the Green's-function method are proportional only to the distance between step edges. Another distinguishing feature of the Green's-function method is that it directly calculates the spectral-density function $\rho(\omega)$, instead of first determining the normal-mode eigenvectors and eigenvalues. Details of this implementation of the Green's-function technique will appear elsewhere.[21] Manipulations (e.g., diagonalization or inversion) of an $N\times N$ matrix require $O(N^3)$ operations, so the computational work increases algebraically with terrace width. As will be seen later in this section, the resulting accuracy increases geometrically with terrace width.

As the terrace width increases, so does the number of surface phonons for each $\bar{Q}$. Most of these are tightly spaced in frequency, generating continuous *surface* bands (in addition to the more familiar *bulk* bands). A few phonons are nondegenerate with these bands, having peeled away from either the bulk or surface modes. This identifies them as step phonons (Fig. 11). Before proceeding, I will clarify the relationship between the phonon

TABLE II. Different types of spectral-density functions. For the third column, the superscript denotes the dimensionality of the integral of the standard output required.

Symbolic notation	Name	Calculation procedure used here
$\rho(\mathbf{Q},\omega)$	bulk	a
$\rho(l_z,l_z';\bar{Q},\omega)$	surface	b
$\rho(L_z;\bar{Q},\omega)$	surface-projected bulk	a^1 or b
$\rho(l_y,l_z;l_y',l_z';Q,\omega)$	edge	c
$\rho(L_y;l_z,l_z';Q,\omega)$	edge-projected surface	b^1
$\rho(L_y,L_z;Q,\omega)$	edge-projected bulk	a^2 or b^1

[a] Diagonalization of 3×3 matrix.
[b] Green's-function method for low-MI surface (Ref. 20).
[c] Green's-function method for high-MI surfaces (as described in Sec. IV).

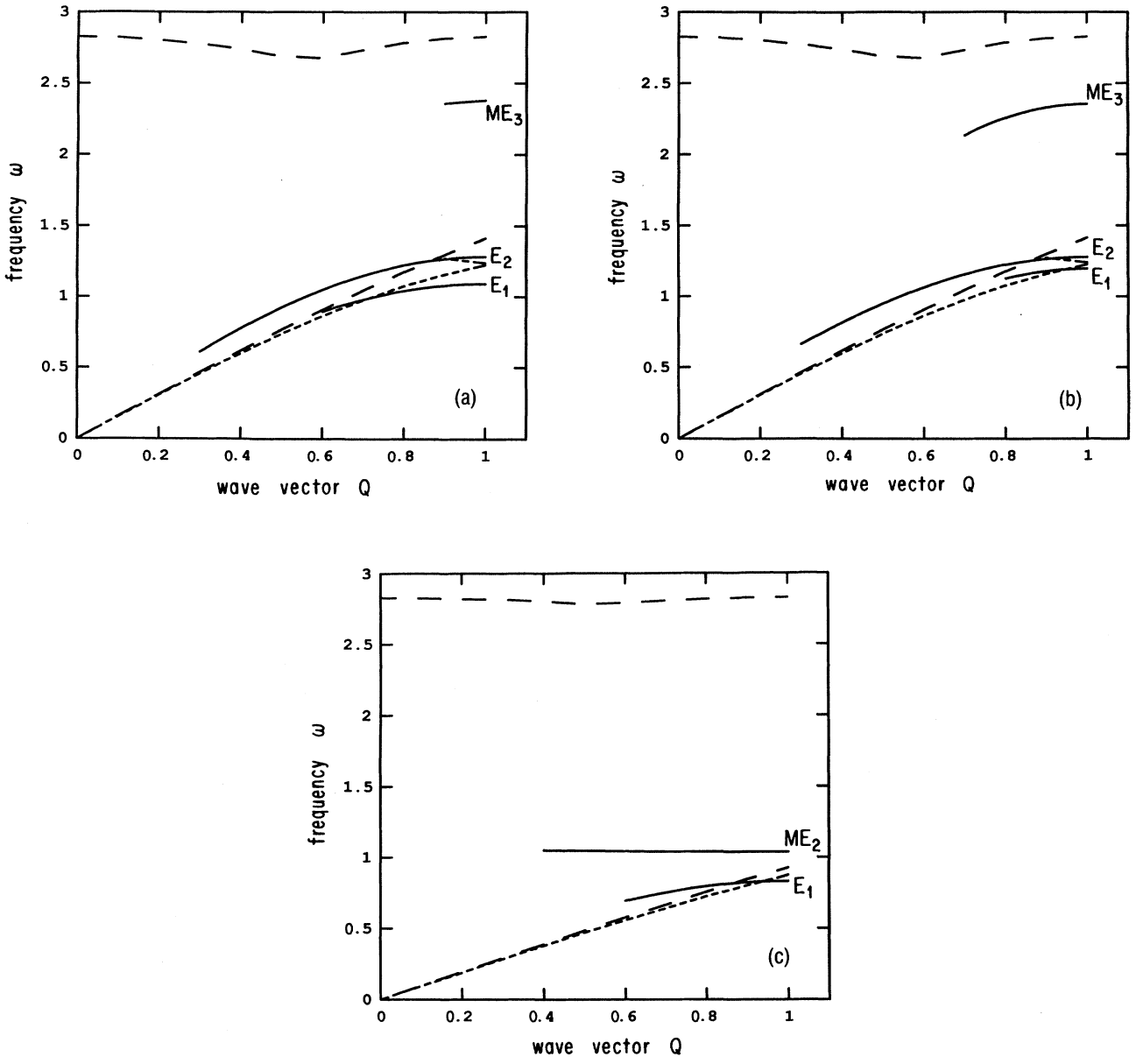

FIG. 10. Schematic diagrams of bulk, surface, and step phonons for systems $A-E$ are presented in (a)–(e), respectively. The bulk and surface bands are bordered by long- and short-dashed lines, respectively. Step phonons (and resonances) are represented by solid lines. The wave vector Q is taken to equal unity at the end of the BZ. Note the absence of any step modes for a type-D system.

eigenvector $[\mathbf{e}(l_z,\bar{Q})]$ for a surface with periodically spaced steps and that for a surface with an isolated step $[\mathbf{e}(l_y,l_z;Q)]$. This will also clarify the relationship between the corresponding spectral densities. The eigenvectors should resemble each other in the limit of wide terraces, but only if the proper mapping is made between the "layer" index l_z and the row indices (l_y,l_z). This simple procedure is illustrated in Fig. 12, by comparing the notation for fcc(755) with that for an isolated A-type step. For instance, $l_z=6$ is mapped to $(l_y,l_z)=(-1,1)$.

All mode characteristics are calculated from $\rho_{\alpha\beta}(l_z,l_z';\bar{Q},\omega)$ using Eq. (4). For instance, the squared amplitude in the αth direction is given by

$$|e_\alpha^{(n)}(l_z,\bar{Q})|^2=\lim_{\epsilon\to 0}\int_{\omega_n(\bar{Q})-\epsilon}^{\omega_n(\bar{Q})+\epsilon} d\omega\,\rho_{\alpha\alpha}(l_z,l_z;\bar{Q},\omega)\ , \tag{9}$$

keeping in mind that for a surface with periodically (but widely) spaced steps [such as fcc(755)], the single index l_z must be used to indicate the position of the (widely spaced sequence of) atomic rows, rather than the ordered

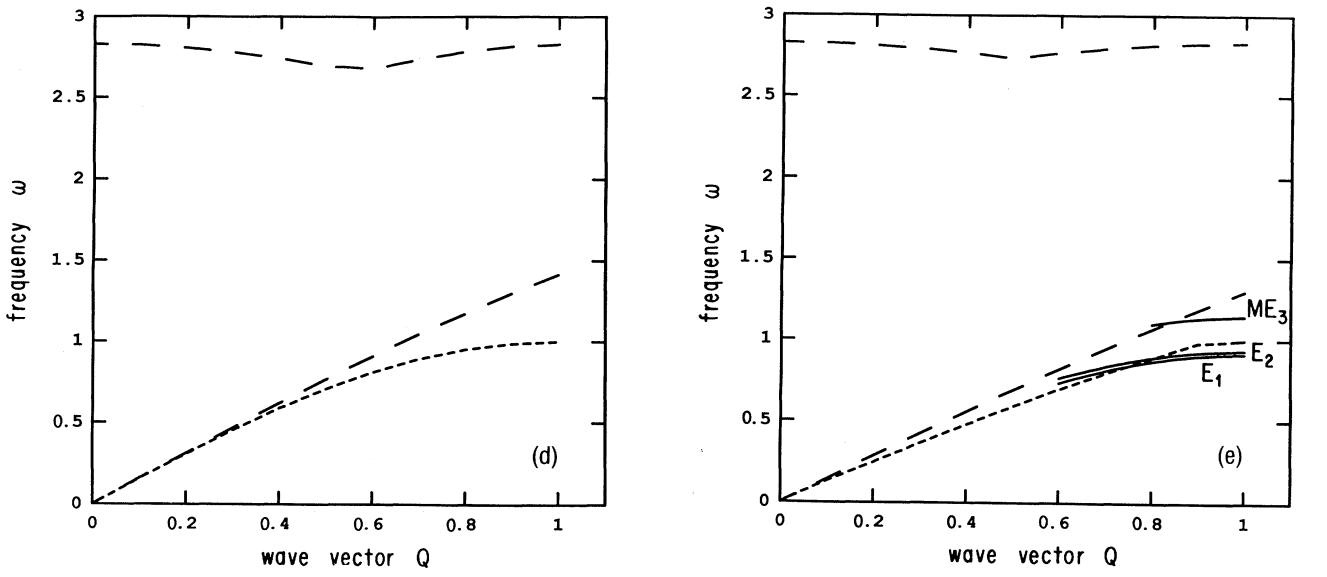

FIG. 10. (*Continued*).

pair (l_y,l_z). As the MI increases, Eq. (9) gets vanishingly small (even for small l_z) for a regular surface phonon, owing to the dilution of its amplitude over the terrace width. For step phonons, however, Eq. (9) approaches a nonzero value when the layer index l_z maps closely enough to the row indices $(l_y,l_z)=(0,0)$. Thus identified, the step-phonon characteristics converge quickly with increasing terrace width. For resonances, this procedure is trickier, because ϵ [in Eq. (9)] must be kept significantly larger than the natural linewidth. If either the linewidth is large or the amplitude is small, the mode characteristics are ill-defined.

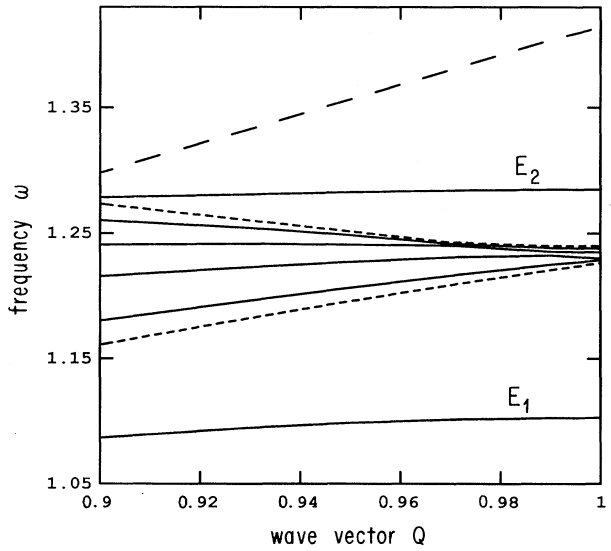

FIG. 11. Enlarged view of a small portion of Fig. 10(a). It additionally includes the dispersion curves (solid lines) for *all* of the surface phonons which exist for fcc(755), featuring four "regular" surface phonons (bounded by short-dashed lines) and two "step" phonons (E_1 and E_2). Note that the regular surface phonons begin to form a continuous band. The narrowness of the surface band at the zone boundary is due to weak dispersion of the Rayleigh mode S_1 in the $[11\bar{2}]$ direction, at that point in the step BZ.

As seen in Fig. 6, the width of the surface BZ decreases as the width of the terrace increases. The step-phonon frequency $\omega(Q_x,Q_y)$ is expected to disperse slightly with Q_y, the wave-vector component *perpendicular* to the step. This shows that step modes localized on neighboring steps may couple weakly with each other by tunneling across the intervening terrace. Although I am concerned mainly with the infinite-terrace-width limit of ω, it is helpful to determine exactly how ω converges, in order to better extrapolate to the final result. By adapting some results for the tight-binding approximation of *electron*

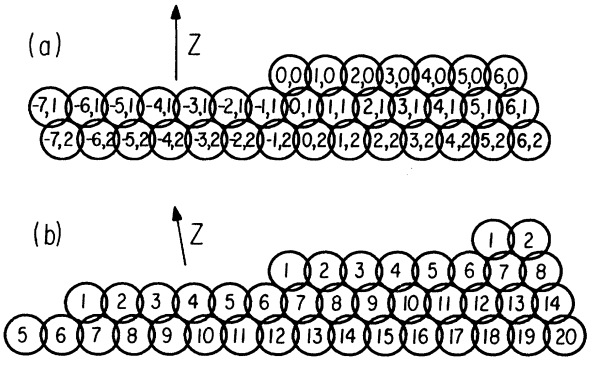

FIG. 12. Comparison of indexing methods for (a) flat surface with one step and (b) fcc(755). These are side views with $[01\bar{1}]$ direction pointing into the page. The circles of the former contain the row indices (l_y,l_z) and those of the latter contain the "layer" index l_z.

TABLE III. Convergence of type-A step-phonon characteristics as terrace width increases.

MI	$\omega(E_1)$	$\lvert E_1\rvert^2$	$\omega(E_2)$	$\lvert E_2\rvert^2$	$\omega(\mathrm{ME}_3)$	$\delta\omega(\mathrm{ME}_3)$	$\lvert \mathrm{ME}_3\rvert^2$
(211)	1.1031	0.582	1.2844	0.805	2.3847	0.0000	0.462
(533)	1.1028	0.581	1.2854	0.778	2.387	0.026	0.435
(322)	1.1028	0.581	1.2850	0.773	2.387	0.015	0.423
(755)	1.1028	0.581	1.2850	0.771	2.383	0.018	0.445

band structure,[22] the limiting behavior of the step-phonon frequency is found to be

$$\omega(Q_x,Q_y,R)-\omega(Q,R=\infty) \simeq ae^{-2R/\lambda}+be^{-R/\lambda}\cos(Q_yR-\delta_1) +ce^{-2R/\lambda}\cos 2(Q_yR-\delta_2)\ , \tag{10}$$

where R is the spacing between steps, λ is the lateral extent of the step phonon, and a, b, and c are on the order of $\sqrt{\phi''/M}$. Similar equations hold for other step-phonon characteristics, like the amplitude and polarization. The specific symmetry of the surface BZ might place certain constraints upon these parameters. For instance, for surfaces with p- or c-rectangular BZ's (i.e., those with mirror symmetry), the phases (δ_1,δ_2) vanish. At the "end" of the surface BZ (i.e., along the dotted lines in Fig. 7), a pair of identities follows simply from the way that the BZ's fit together to fill momentum space and from the smoothness of $\omega(\bar{Q})$. For c-rectangular BZ's, b vanishes. For p-oblique BZ's, the phases (δ_1,δ_2) are equal to each other and specified by the symmetry of the right side of Eq. (8) with respect to reflection through the point midway between $\bar{A}$ and $\bar{B}$. The second term in Eq. (10) decays more slowly with R than the others so the fastest convergence occurs by setting either $Q_yR-\delta_1=\pm\pi/2$ or $b=0$, if possible. Accordingly, calculations were made to obtain easily the infinite-terrace-width limit of the step-phonon characteristics.

Before presenting results, it is worth justifying the omission of surfaces with nonuniform terrace widths, as specified towards the end of Sec. II. I use fcc(337) as an example of such an A-type surface. Adjacent steps on fcc(337) have slightly dissimilar environments, of two different types. This leads to two modes of slightly differing frequencies, corresponding to different linear combinations of vibrational amplitude at either edge. The step modes of fcc$(2N-1,2N-1,2N+3)$ will converge to the correct results as $N\to\infty$, but require a factor of $2^3=8$ increase in computations, thereby indicating their undesirability for the main task of this paper, which is the determination of step-phonon characteristics for a completely isolated step.

V. RESULTS

A. (111) terrace with (001) step face

Near the end of the BZ, three step modes exist, including one gap step phonon (E_2) and one resonance (ME_3). The mode nomenclature is analogous to that introduced in Ref. 5 for surface phonons. E and ME stands for edge and mixed edge, respectively. Table III indicates that the step-phonon characteristics converge rapidly as the terrace width increases from 2 to 5 atomic rows. The polarization of the step modes varies from row to row, but at the step edge (where the amplitude peaks) E_1 and E_2 are transverse (to the direction of propagation) and ME_3 is longitudinal. Although neither transverse mode is either shear horizontal (i.e., perpendicular to step and parallel to surface) or shear vertical, E_1 and E_2 are, respectively, polarized parallel and perpendicular to the step *face* (Table V). In this and all subsequent tables, the quantity $\lvert E_j\rvert^2$ indicates the squared amplitude of the jth step phonon, evaluated at the step edge. The square amplitude is normalized to unity over the entire crystal; hence it would equal unity for a step mode completely localized at the row of edge atoms, but vanish instead for a bulk or surface mode. The localization properties for typical step, surface, and bulk modes are presented graphically in Fig. 13.

As Q moves more than 10% away from the end of the BZ [Fig. 10(a)], ME_3 loses its enhanced step (and surface) localization, and E_2 becomes degenerate with bulk modes, transforming into a step resonance (ME_2). E_1 retains its localization properties over a longer portion of the BZ, but no mode is even resonantly step-localized near $Q=0$. For all of the step modes seen (on this and other types of step), the polarizations depend only weakly upon both Q and the terrace width.

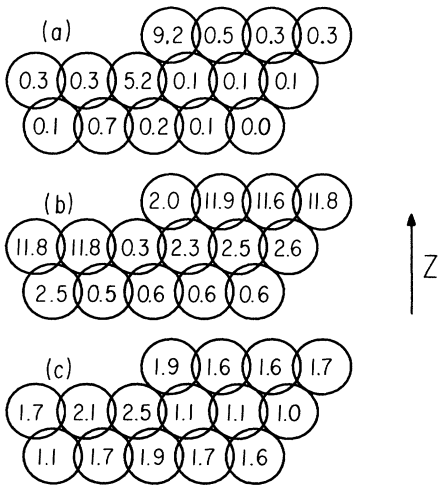

FIG. 13. Spatial dependence of the squared vibrational amplitude near an A-type step, as manifested by the edge spectral density $\rho(l_y=l_y',l_z=l_z';Q,\omega)$. The wave vector Q is taken at the end of the step BZ. This behavior differs markedly for (a) E_1 step phonon ($\omega=1.10$), (b) S_1 surface phonon ($\omega=1.23$), and (c) bulk phonon ($\omega=1.50$).

TABLE IV. Convergence of type-B step-phonon characteristics as terrace width increases.

MI	$\omega(E_1)$	$\lvert E_1\rvert^2$	$\omega(E_2)$	$\lvert E_2\rvert^2$	$\omega(\mathrm{ME}_3)$	$\delta\omega(\mathrm{ME}_3)$	$\lvert \mathrm{ME}_3\rvert^2$
(110)	1.1996	0.795	1.3164	0.848	2.4016	0.000	0.679
(331)	1.2080	0.743	1.2876	0.803	2.3515	0.000	0.606
(221)	1.2074	0.730	1.2881	0.790	2.3606	0.000	0.587
(553)	1.2081	0.739	1.2871	0.774	2.3483	0.002	0.600
(332)	1.2081	0.739	1.2871	0.771	2.353	0.027	0.753
(775)	1.2081	0.739	1.2871	0.770	2.349	0.004	0.569

B. (111) terrace with $(11\bar{1})$ step face

The results for this step resemble those of the previous system. Three step phonons exist, including one gap mode and one resonance. At the edge, their polarizations virtually duplicate those of A, but because the step-face orientations differ for A and B, the modes E_1 and E_2 are no longer polarized in directions parallel or perpendicular to either the step face or the terrace. The polarization vector of E_1 lies in the plane bisecting those of the terrace and step face. The step-phonon frequencies are quite similar to those of the type-A system. The main difference is that E_1 lies much closer to the surface band. As a result, E_1 is a true step mode only within $<10\%$ of the end of the BZ [Fig. 10(b)]. One surprising limit to note is the swift convergence of the step-phonon characteristics with increasing MI (Table IV).

The similarity between the converged results and those for fcc(110) is quite surprising, considering that the latter is not usually considered to be a vicinal surface. The numbers in the first row of Table IV refer to the three *surface* modes commonly known as S_1, S_2, and S_7, which have been studied both theoretically and experimentally. More will be said about this in Sec. VI.

TABLE V. Converged characteristics of zone-boundary step phonons.

Stepped surface	Mode	Frequency	Approximate polarization	$\lvert E\rvert^2$ (step localization)
A	E_1	1.103	[110] transverse	0.58
	E_2	1.285	[001] transverse	0.77
	ME_3	2.38	$[1\bar{1}0]$ longitudinal	0.44
B	E_1	1.208	[110] transverse	0.74
	E_2	1.287	[001] transverse	0.77
	ME_3	2.35	$[1\bar{1}0]$ longitudinal	0.6
C	E_1	0.842	[320] mixture	0.25
	ME_2	1.00±0.05	$[01\bar{1}]$ mixture	0.4
D			no step modes	
E	E_1	0.925	[001] longitudinal	0.41
	E_2	0.938	[010] shear horizontal	0.44
	ME_3	1.12±0.04	[100] vertical	0.4

C. Other steps

Similar behavior is seen for two of the other three classes of stepped surface. For a type-C step, only one step mode (E_1) exists, and it is not very strongly localized to the edge. As a result, its characteristics do not converge as rapidly as those for other step modes. The polarization of E_1 is elliptical for small terrace widths but becomes essentially linear (like the other step modes) as the MI increases. Its polarization is neither longitudinal nor transverse. Owing to the proximity of both the bulk and the surface bands, E_1 does not survive very far away from the end of the BZ [Fig. 10(c)]. In addition, one broad step resonance (ME_2) appears, polarized in a direction not quite perpendicular to that of E_1.

No true step phonons exist for a D-type system [Fig. 10(d)], at least not without modification of the present very simple force-constant model. I examined surfaces having MI's of the form $(1\,1\,N)$, with $N=5$, 7, 9, 11, and 13.

Two step phonons exist for a type-E system. At the zone boundary, E_1 and E_2 are almost degenerate. E_1 is polarized longitudinally and E_2 shear horizontally. Additionally, a shear vertically polarized step resonance (ME_3) is evident, although fairly broad. All three modes exhibit step-localization properties only near the end of the BZ [Fig. 10(e)].

D. Summary of results

For systems A and B, two true step phonons are evident for each, as reported in Ref. 11. Two such modes are also seen for step E, but only one exists for step C, and none are seen for D. An additional resonance appears for each step except D. Hence three mutually orthogonal step modes (or resonances) appear for A, B, and E. This is consistent with what would occur if the atoms not along the edge were infinitely massive (i.e., frozen in place). In that situation, there would be exactly three step modes, all mutually orthogonal and completely localized to the step edge. The substrate flexibility alters this picture quantitatively for A, B, and E. It is unclear why this simplistic interpretation also fails *qualitatively* for C and D. Table V summarizes the step-phonon characteristics for all five systems.

To summarize these results, it is worth making several comparisons and contrasts between step modes on vicinal surfaces and surface modes on flat surfaces. As for sur-

face phonons on flat surfaces, when the step-phonon dispersion pierces a bulk band, a step resonance appears as a continuation. When a step phonon penetrates a surface band (but remains nondegenerate with a *bulk* band), the step resonance manifests itself as one (or more) surface phonon(s) with very large amplitude at the edge, a behavior analogous to that of a pseudosurface mode output by a slab calculation.[5] Hence, in certain circumstances, a step resonance represents the decay of a step mode to a surface mode, but not to a bulk mode. On the (100) and (110) surfaces of certain fcc crystals, certain vibrational modes are seen (numerically) to localize in layers near, but not restricted to, the topmost one. This phenomenon is a direct result of the ability of such single-layer modes to persist deep in the bulk. No analogous single-row modes exist for fcc crystals; hence no step phonons are expected to localize in a row near, but not restricted to, the edge. Accordingly, none are seen. On flat surfaces, one surface phonon exists over the entire surface BZ, all of the way to $\bar{Q}=\bar{\Gamma}$. The long-wavelength characteristics of this mode, the Rayleigh wave, are derived from elastic theory. In particular, its z-attenuation length is inversely proportional to $|\bar{Q}|$. Similar arguments can be used to discuss the possibility of a long-wave, low-frequency step mode, expected to exhibit z- and y-attenuation lengths inversely proportional to Q. However, when these attenuation lengths significantly exceed one atomic spacing (the size of the step), this diluted mode is not expected to view the monatomic step as a defect which is strong enough to localize vibrations. This prevents the occurrence of such acoustic step waves; none are seen. Finally, no step mode is degenerate with a bulk or surface band but decoupled from it by symmetry. This is because such decoupling could only occur at $Q=0$ (see end of Sec. III), a portion of the BZ where, it has just been shown, no step modes exist.

E. Dependence upon the force-constant model

Both step and surface phonons are sensitive to changes in the near-surface force constants. One such possible variation is a nonzero value of surface stress, meaning that $\phi'\neq 0$ [see Eq. (2)] between atoms on the surface. The phonon frequencies vary monotonically with surface stress, whether it be positive (attractive or tensile) or negative (expansive) (Fig. 14). However, step phonons and surface phonons differ in their sensitivity to changes in the near-*edge* force-constant model, for obvious reasons. For instance, if $\phi'\neq 0$ between atoms along the step edge (akin to tension in a string), a substantial monotonic dependence occurs in the frequencies of transversely polarized step phonons, though not for surface phonons or longitudinally polarized step phonons (Fig. 15). In fact, a step phonon appears on step D by peeling away from the bottom of the surface band, if even an infinitesimally small amount of negative edge tension is applied. Another possible variation is in the near-surface spring constant ϕ''. If this quantity is allowed to vary only along the step edge, a substantial monotonic dependence occurs in the frequency of *longitudinally* polarized step phonons, though not for surface modes or transversely polarized step modes (Fig. 16).

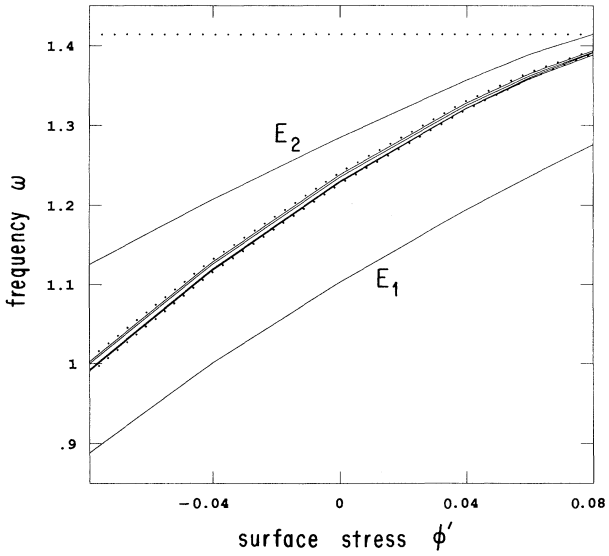

FIG. 14. Surface-phonon frequencies for fcc(755) at $\bar{Q}=\bar{S}$, as functions of surface stress ϕ'. The units of ϕ' are taken proportional to $r_0\phi''$. These were calculated in the partial harmonic approximation of Ref. 5. The upper dotted line depicts the lower boundary of the bulk band. The lower two dotted lines, enclosing the tightly spaced sequence of four regular surface modes, represent the surface band boundaries [as calculated from Eq. (8)].

Nickel forms an fcc lattice whose bulk-phonon spectra are fit well (better than any other element) by the simple single force-constant model.[23] Surface-phonon measurements for the low-MI surfaces (100),[18,24] (110),[24] and (111) (Ref. 25) indicate varying amounts of surface intralayer force-constant softening ($\phi''_{\text{surf}}<\phi''_{\text{bulk}}$) and tensile stress

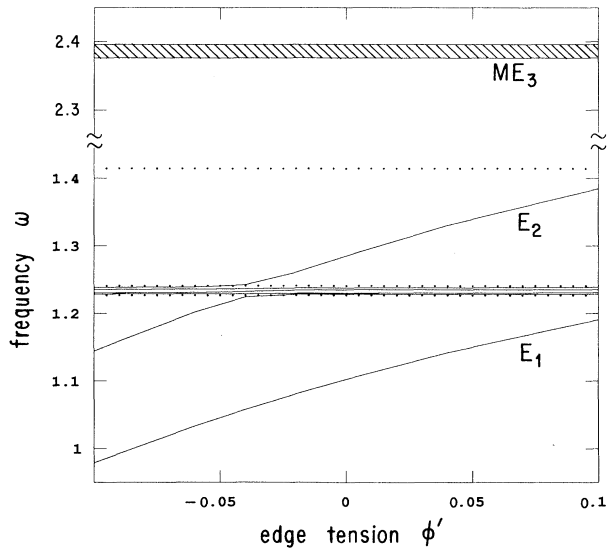

FIG. 15. Same as Fig. 14, but for stress confined to the step edge. In this case, the partial and full harmonic approximations coincide.

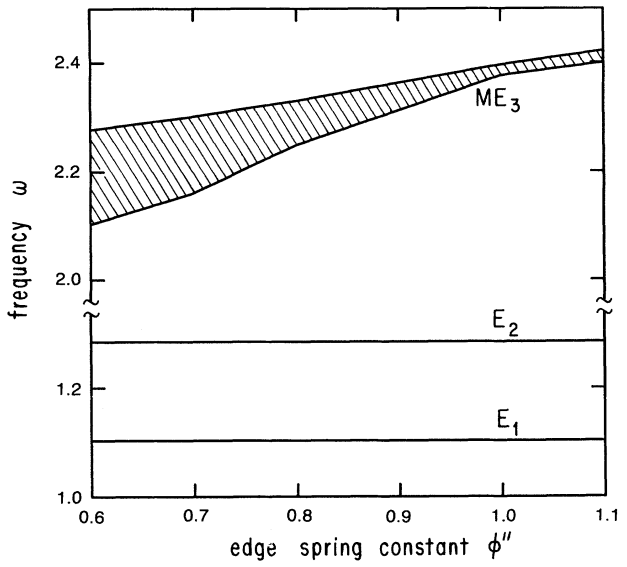

FIG. 16. Step-phonon frequencies for fcc(755) at $\bar{Q}=\bar{S}$, for spring-constant deviation $\delta\phi''$ confined to the step edge.

($\phi'_{\text{surf}}>0$). Hence a preliminary study of the vibrational properties of a stepped nickel crystal surface should incorporate these changes. This has been accomplished for Ni(755), yielding results quite similar to those in Fig. 10(a). One key aspect of this will be discussed in the next section.

The adsorption of atoms or molecules onto a stepped surface will alter the results presented in this paper for two reasons. First, the different mass and bonding strength of the adparticle will grossly change the near-surface Hamiltonian, perhaps generating modes localized largely to the adlayer. Second, the adparticles will induce chemical changes affecting the substrate-substrate interaction, thereby altering the characteristics of preexisting surface and step modes. Although I present no calculations for adlayers on stepped surfaces, a few obvious developments are worth anticipating. If the coverage is substantial (>0.25 monolayer), both surface and step mode characteristics will change, depending on the specifics of the adsorbate mass, adsorption strength, etc. If the coverage is small, the particles might arrange themselves along the step rather than on the terrace. In this situation, the surface phonons will remain unchanged, but not so for step phonons. For instance, a line of light atoms adsorbed along a step will generate three high-frequency step modes with amplitude largely restricted to the adatoms. If the adatom-adatom interaction is strong enough, dispersion (with Q) will occur, especially for the longitudinally polarized mode. The characteristics of these phonons will tell much about the adatom-step interaction.

VI. EXPERIMENTAL ASPECTS

Only two inelastic-scattering experiments[10,13] have been performed on crystals with widely separated steps. Both were EELS experiments performed at or near $\bar{Q}=\bar{\Gamma}$, and each detected one step phonon. Their proximity to $\bar{\Gamma}$ indicates that they do not coincide with any of the step phonons covered in this paper, for reasons discussed at the end of Sec. V D. In fact, both experimental results seem to require a modification of the near-edge force-constant model in order to correctly predict the existence of the observed modes.

The first of these experiments[13] was on Pt(332), a type-A system with edge separation of 13 Å. In specular geometry, a vibrational mode at 25.4 meV was detected, significantly exceeding the phonon frequencies of both Pt(111) and bulk platinum. This is a surprising result, because Rayleigh's theorem predicts that step-phonon frequencies should fall *below* bulk and surface bands.[7] Subsequent explanations for the vibrational mode linked this anomaly to force constants which are substantially stiffened near a step edge.[26,27] This is not inconsistent with the mode's dipole activity (as indicated by the large cross section near $\bar{\Gamma}$), which is due to a large fractional charge transfer to the step Pt atom.

The second experiment[10] was on TiC(310), a metallic compound with steps separated by about 7 Å. Since this polyatomic material forms a rocksalt structure, its phonons differ greatly from those of the monatomic fcc materials considered here. A band of several folded surface modes was seen. Near $\bar{\Gamma}$, a mode was seen at $\Delta E=18$ meV, well below the surface band. The existence of this step phonon could be explained only by decreasing a certain edge force constant by 40%, in contrast with the Pt(332) results.

Now I will discuss the possibility of detecting, with either EELS or HAS, the step phonons analyzed in this paper. One might view fcc(110) as a stepped surface, with (111) terraces and (11$\bar{1}$) step faces. Geometrically this is a weak argument, because the terraces are only one atomic row wide. However, Table III shows that fcc(110) surface phonons S_1, S_2, and S_7 have characteristics extremely close to their converged *step*-phonon counterparts E_1, E_2 and ME_3, respectively. There is ample experimental evidence for these three surface phonons. The mode S_1 has been seen on Ni(110),[24] Ag(110),[28] and Al(110),[29] in each case with a frequency slightly higher than expected for E_1. The mode S_2 has been seen only on Ni(110),[24] with a frequency corresponding exactly to that for E_2. The frequencies of S_7 detected on Ni(110) (Ref. 24) and Cu(110) (Ref. 30) are slightly lower than expected for ME_3. Hence it might be argued that these "detections" of E_1, E_2, and ME_3 indicate slight amounts of tensile stress ($\phi'>0$) and softening ($\delta\phi''<0$) along the steps. To be more convincing, however, evidence of this type of step phonon should probably come from a surface with wider terraces.

A good candidate for observing step phonons should exhibit modes which have a large amplitude of shear vertical polarization in the top layer and which are well separated (in energy) from any other vibrational features which might appear brightly in the spectrum (such as bands of surface or bulk phonons). This leads to the most logical choice of E_1 on a type-A stepped surface [e.g., Ni(755)]. A difficulty with this experiment is that the step-phonon intensity would vary linearly with the densi-

ty of step edges, i.e., inversely with terrace width. On the other hand, the surface- (and bulk-) phonon intensities would remain roughly constant, thereby presenting a (comparatively) large background to the step-phonon peak. Unfortunately, no experimental technique exists that is sensitive to vibrations *only* in the vicinity of steps.

To be sufficiently predictive, a multiple-scattering calculation should be performed. This has been accomplished with reasonable success for both EELS (Ref. 31) and HAS,[32] but only for low-MI surfaces, and lies beyond the scope of this paper. Problems appear in extending these methods to stepped surfaces.[33] For instance, the rigid-ion multiple-scattering (RIMS) method for calculating EELS intensities requires the inversion of matrices with size roughly proportional to the number of LEED spots, which increases linearly with the terrace width. This linear-algebra difficulty, comparable to those faced in the lattice dynamics of this paper, is surmounted by simply allowing for longer computing time. A more serious problem lies in the small interlayer spacing [=0.35 Å for Ni(755)]. Traditional k-space methods (i.e., using a plane-wave basis for the electron being scattered) require the interlayer spacing to exceed 1 Å in order to converge. However, a new L-space method (i.e., using a spherical-wave basis) for LEED calculations is especially well suited for stepped surfaces.[34] This should prove useful for EELS calculations as well.

It is possible to estimate crudely the inelastic-scattering intensity from such a stepped surface, for which I will use Ni(755) as an example. In the one-phonon approximation (i.e., ignoring multiphonon processes), the intensity from *all* vibrational modes (i.e., bulk, surface, and step) is proportional to[19]

$$I(\mathbf{k}_i,\mathbf{k}_f)=\frac{1}{\omega(1-e^{-\hbar\omega/k_BT})}\times\sum_{\alpha,\beta,l_z,l_z'}A_\alpha(l_z;\mathbf{k}_i,\mathbf{k}_f)A_\beta^*(l_z';\mathbf{k}_i,\mathbf{k}_f)\times\rho_{\alpha\beta}(l_z,l_z';\bar{Q},\omega)\ , \tag{11}$$

where the initial and final wave vectors of the impinging particle are $\mathbf{k}_i$ and $\mathbf{k}_f$, the parallel momentum transfer is $\bar{Q}=\bar{k}_i-\bar{k}_f$, and the energy transfer is $\hbar\omega=\hbar^2(|\mathbf{k}_i|^2-|\mathbf{k}_f|^2)/2m$, where m is the particle mass. The inelastic matrix elements $\mathbf{A}(l_z;\mathbf{k}_i,\mathbf{k}_f)$ derive from a multiple-scattering calculation (as have been done for low-MI surfaces for both EELS and HAS) not to be performed here. One crude, but perhaps useful, approximation for the inelastic matrix elements is

$$\mathbf{A}(l_z;\mathbf{k}_i,\mathbf{k}_f)=\begin{cases}\hat{\mathbf{z}}A(\mathbf{k}_i,\mathbf{k}_f) & \text{if } l_z\le N\\ 0 & \text{otherwise}\ ,\end{cases} \tag{12}$$

where N is the number of rows in the terrace [$\simeq 6$ for fcc(755)]. Equation (12) makes three assumptions, some more reliable than others. First, it assumes that only shear vertical motion is important (reasonable for typical HAS and EELS geometries). Second, it assumes the inelastic scattering to occur in the top terrace layer only (correct for HAS, but less so for EELS). Third, it assumes that all top layer atoms scatter equivalently (only true when fairly well removed from the step edge). Hence the estimated intensity is proportional to

$$[\omega(1-e^{\hbar\omega/k_BT})]^{-1}\sum_{l_z l_z'}^{N}\rho_{zz}(l_z,l_z';\bar{Q},\omega)\ .$$

This approach has been applied to Ni(755) for Q taken near the end of the (first) BZ, showing that E_1 might be detectable (Fig. 17). An actual experiment would presumably depart from this estimate, depending strongly on both $\mathbf{k}_i$ and $\mathbf{k}_f$; nevertheless, its average spectrum is expected to resemble this. Future EELS or HAS calculations should help by finding experimental windows within which the intensity ratio of step phonon to (bulk phonons plus surface phonons) is enhanced by perhaps a factor of 10 over the ratio ($\sim$40%) seen in Fig. 17. This procedure has been used quite effectively in optimizing EELS intensity from *surface* phonons on flat surfaces.[17,25,31]

VII. CONCLUSION

In summary, I have systematically explored the localization properties of phonons near stepped surfaces of five different types, employing a very basic force-constant model. The number of surface modes increases linearly

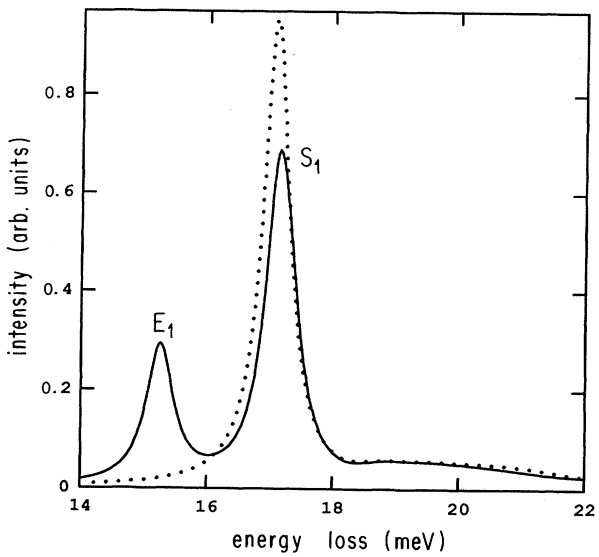

FIG. 17. Crude estimate of the energy-loss spectrum for Ni(755) (solid line) and the comparable quantity $[\omega(1-e^{-\hbar\omega/k_BT})]^{-1}\rho_{zz}(l_z=l_z'=1;\bar{Q},\omega)$ for Ni(111) (dotted curve). This is done near the end of the first BZ, i.e., $Q\sim 1.26$ Å^{-1}. The peak at $\Delta E\sim 17.1$ meV is due to the Rayleigh surface mode, polarized mainly shear vertically, whereas the peak at $\Delta E\sim 15.2$ meV is due to the step mode E_1. No strong features appear outside this range of energy loss. These functions are taken at constant $\bar{Q}$, meaning that the scan curve is vertical, not realistic for HAS (e.g., see Fig. 39 of Ref. 4). However, the result for a realistic scan curve should only differ quantitatively from this figure.

with terrace width, most of which coalesce to form continuous bands. However, a small number of these might localize to the step, which should itself be viewed as a defect. In four of the five systems considered, the defect is strong enough to generate such modes, but only near the end of the step BZ. A simplistic "frozen substrate" explanation predicts the existence of a total of three mutually orthogonal step modes (and resonances). This interpretation qualitatively succeeds for steps *A*, *B*, and *E*, but not for *C* or *D*. Step phonons are sensitive to changes in the near-step interatomic potential. Accordingly, two previous step mode measurements have yielded information about that important region of the crystal surface. I propose a third such experiment, with Ni(755), a possibly simpler system than those previously studied.

Note added in proof. A recent HAS experiment on Al(221) by Lock, Toennies, and Witte[35] seems to detect step phonons for this *B*-type surface.

ACKNOWLEDGMENTS

I am indebted to Professor Ugo Fano and Professor Steven Sibener for guidance throughout this project, and for critical readings of the manuscript. I also thank Francis Robicheaux, Dan Koleske, and Professor Talat Rahman for carefully proofreading this paper. I gratefully acknowledge conversations with Dr. Burl Hall, Professor John Black, and Professor J. M. Blakely. I thank R. Michael Townsend for help with the computer programming. This research was supported by the National Science Foundation Materials Research Laboratory at The University of Chicago.

APPENDIX: KINK MODES

Near an isolated kink in a step on an otherwise flat surface there are no translational periodicities which separate the Hamiltonian into components corresponding to different phonon momenta. For a monatomic crystal, the bulk-phonon band ranges continuously from 0 (acoustic modes) to $\omega_{\max}$ ($=2\sqrt{2}\sqrt{\phi''/M}$ for the present model). A phonon can truly localize to the kink only if nondegenerate with the bulk band, i.e., if its frequency exceeds $\omega_{\max}$. However, Rayleigh's theory predicts that the kink mode frequency must fall *below* bulk, surface, and step bands, in the absence of sizable stiffening of force constants near the kink.[7] Thus only two circumstances allow for the possibility of one (or more) kink modes. One requires substantial stiffening of near-kink force constants, a quite plausible situation. The other requires the crystal to be polyatomic, so that gaps might appear in the bulk density of states, separating acoustic from optical bands. For discussion purposes, I will assume that this latter circumstance holds. Roughly speaking, if the polyatomic mass ratio is large, so is the gap. The upper band(s) consists of motion restricted almost entirely to the light atoms, and the lower band involves motion of both (all) types of atoms. Take LiI as an example. This rocksalt structure has a mass ratio of 18:1. If a kink in a step on a LiI surface consists of a lithium atom, a kink mode probably results. The mode involves motion of predominantly the single light atom, and the frequency falls below the bands of bulk, surface, and step vibrations of lithium.

---

*Present address: Naval Research Laboratory, Mail Code 6877, Washington, D.C. 20375-5000.

[1]Elliott W. Montroll and Renfrey B. Potts, Phys. Rev. **102**, 72 (1956).

[2]H. Ibach and D. L. Mills, *Electron Energy Loss Spectroscopy and Surface Vibrations* (Academic, New York, 1982).

[3]R. B. Doak, U. Harten, and J. P. Toennies, Phys. Rev. Lett. **51**, 578 (1983).

[4]K. D. Gibson and S. J. Sibener, J. Chem. Phys. **88**, 7862 (1988).

[5]R. F. Allen, G. P. Alldredge, and F. W. deWette, Phys. Rev. B **4**, 1648 (1971); and following paper.

[6]For a recent review see J. E. Black, *Structure and Dynamics of Surface I,* edited by W. Schommers and P. von Blankenhagen (Springer-Verlag, Berlin, 1986), p. 153.

[7]A. A. Maradudin, E. W.Montroll, G. H. Weiss, and I. P. Ipatova, *Theory of Lattice Dynamics in the Harmonic Approximation* (Academic, New York, 1971).

[8]J. E. Black and P. Bopp, Surf. Sci. **140**, 275 (1984).

[9]G. Armand and P. Masri, Surf. Sci. **130**, 89 (1983).

[10]M. Wuttig, C. Oshima, T. Aizawa, R. Souda, S. Otami, and Y. Ishizawa, Surf. Sci. **193**, 180 (1988).

[11]P. Knipp, Phys. Rev. B **40**, 7993 (1989).

[12]A. A. Maradudin, R. F. Wallis, D. L. Mills, and R. L. Ballard, Phys. Rev. B **6**, 1106 (1972).

[13]H. Ibach and D. Bruchmann, Phys. Rev. Lett. **41**, 958 (1978).

[14]P. Masri, G. Allan, and L. Dobrzynski, J. Phys. (Paris) **33**, 85 (1972).

[15]B. Lang, R. W. Joyner, and G. A. Somorjai, Surf. Sci. **30**, 440 (1972); Gabor A. Somorjai, *Chemistry in Two Dimensions: Surfaces* (Cornell University, Ithaca, 1981).

[16]H. V. Thapliyal, Ph.D. thesis, Cornell University, 1977; J. M. Blakely and H. V. Thapliyal, in *ASM Seminar on Interfacial Segregation,* edited by W. C. Johnson and J. M. Blakely (American Society for Metals, Cleveland, 1979), pp. 137–174.

[17]B. M. Hall, D. L. Mills, Mohammed H. Mohammed, and L. L. Kesmodel, Phys. Rev. B **38**, 5856 (1988).

[18]S. Lehwald, J. M. Szeftel, H. Ibach, T. S. Rahman, and D. L. Mills, Phys. Rev. Lett. **50**, 518 (1983).

[19]P. Knipp and Burl M. Hall, Surf. Sci. **224**, L983 (1989).

[20]J. E. Black, Talat S. Rahman, and D. L. Mills, Phys. Rev. B **27**, 4072 (1983).

[21]P. Knipp (unpublished).

[22]Neil W. Ashcroft and N. David Mermin, *Solid State Physics* (Holt, Rinehart, and Winston, Philadelphia, 1976), Eq. 10.15.

[23]R. J. Birgeneau, J. Cordes, G. Dolling, and A. D. B. Woods, Phys. Rev. **136**, A1359 (1964).

[24]S. Lehwald, F. Wolf, H. Ibach, Burl M. Hall, and D. L. Mills, Surf. Sci. **192**, 131 (1987).

[25]W. Menezes, P. Knipp, G. Tisdale, and S. J. Sibener, Phys. Rev. B **41**, 5648 (1990).

[26]Mark Mostoller and Uzi Landmann, Phys. Rev. B **20**, 1755 (1979).
[27]G. Allan, Surf. Sci. **85**, 37 (1979).
[28]G. Bracco, R. Tatarek, F. Tommasini, U. Linke, and M. Persson, Phys. Rev. B **36**, 2928 (1987).
[29]J. P. Toennies and Ch. Wöll, Phys. Rev. B **36**, 4475 (1987).
[30]P. Zeppenfeld, K. Kern, R. David, K. Kuhnke, and G. Comsa, Phys. Rev. B **38**, 12 329 (1988).
[31]Mu-Liang Xu, B. M. Hall, S. Y. Tong, M. Rocca, H. Ibach, S. Lehwald, and J. E. Black, Phys. Rev. Lett. **54**, 1171 (1985).
[32]V. Bortolani, A. Franchini, F. Nizzoli, and G. Santoro, Phys. Rev. Lett. **52**, 429 (1984).
[33]Burl M. Hall, Ph.D. thesis, University of Wisconsin-Milwaukee, 1983; and private communication.
[34]X.-G. Zhang, P. J. Rous, J. M. Maclaren, A. Gonis, M. A. Van Hove, and G. A. Somorjai, Surf. Sci. **239**, 103 (1990).
[35]A. Lock, J. P. Toennies, and G. Witte, J. Electron Spectrosc. **54/55**, 309 (1990).